Calibration and test of a hyperspectral imaging prototype for intra-operative surgical assistance

Dorra Nouri, Yves Lucas, Sylvie Treuillet

Calibration and test of a hyperspectral imaging prototype for intra-operative surgical assistance

Dorra Nouri*[a], Yves Lucas[a], Sylvie Treuillet[b]
[a]Laboratoire PRISME, IUT Bourges, Université d'Orléans, 63 avenue de Lattre de Tassigny, 18020 Bourges cedex France;
[b]Laboratoire PRISME, Polytech' Orléans, Université d'Orléans, 12 rue de Blois BP 6744, 45067 Orléans cedex 2 France

ABSTRACT

A significant recent breakthrough in medical imaging is the development of a new non-invasive modality based on multispectral and hyperspectral imaging that can be easily integrated in the operating room. This technology consists of collecting series of images at wavelength intervals of only few nanometers and in which single pixels have spectral information content relevant to the scene under observation. Before becoming of practical interest for the clinician, such system should meet important requirements. Firstly, it should enable real reflectance measurements and high quality images to dispose of valuable physical data after spatial and spectral calibration. Secondly, quick band pass scanning and a smart interface are needed for intra-operative mode. Finally, experimentation is required to develop expert knowledge for hyperspectral image interpretation and result display on RGB screens, to assist the surgeon with tissue detection and diagnostic capabilities during an intervention. This paper is focused mainly on the two first specifications of this methodology applied to a liquid crystal tunable filter (LCTF) based visible and near infrared spectral imaging system. The system consists of an illumination unit and a spectral imager that includes a monochrome camera, two LCTFs and a fixed focal lens. It also involves a computer with the data acquisition software. The system can capture hyperspectral images in the spectral range of 400 – 1100 nm. Results of preclinical experiments indicated that anatomical tissues can be distinguished especially in near infrared bands. This promises a great capability of hyperspectral imaging to bring efficient assistance for surgeons.

Keywords: hyperspectral imaging, spatial calibration, spectral calibration, LCTF

1. INTRODUCTION

Starting from the early 1970s, a large number of spaceborne multispectral sensors have been launched. Over the past decade multispectral imaging (MSI) and hyperspectral imaging (HSI) have matured not only in remote sensing field[8, 18] but also in many other fields like food industry[3, 19], biology[9, 6] and recently in the medical field of surgery[1, 17, 20]. HSI and MSI systems both have undergone tremendous conception evolutions in recent years. A simple and low cost approach consists in placing a filter wheel in front of the camera lens, but the number of bands is limited and fixed and a mechanical interface is needed for the wheel rotation[7, 5]. Another technique called push-broom is based on a spectrometer to obtain the complete spectral information but only one imaged line is captured at a time and the field of view must be scanned using a motion device or mirrors[2]. Micro-electro-mechanical systems (MEMS) have recently been introduced[4] to suppress optical and mechanical parts but only visible band sensors have been interfaced at the moment. In a last approach, the spectra response of the lighting device is controlled to select relevant wavelengths but ambient light should be discarded[12].

We opted for an enhanced and innovative version of the first approach where the filter wheel is replaced by an electronically programmable filter system. This can be achieved using liquid crystal tunable filters[11] (LCTF) or acousto-optic filters[16] (AOTF). The major drawback of these filters resides in light attenuation, but flexibility, instantaneous and continuously wavelength selection is essential when designing a HSI or a MSI system for medical applications.

*dorra.nouri@univ-orleans.fr; phone (0033) 248238218

We have developed a LCTF based spectral imaging system in visible and near infrared range. The first section of this paper describes our HSI system overview and its hardware and software integration. Then, we present and detail the methodology used in the spatial and spectral calibration of the HSI system. The results of the calibration and the preclinical experiments are provided and discussed in the final section.

2. MATERIAL AND METHODOLOGY

2.1 Hyperspectral system overview

Our hyperspectral system consists of an illumination system, a spectral imager and a computer with data acquisition software. In order to reduce the cost and time for developing the system, we had selected off-the-shelf commercial products to design our LCTF-based spectral imaging system. The illumination system consists of focused and powerful halogen lighting. The spectral imager is operative in the spectral range of 400 –1100 nm. It is assembled from two LCTFs with 7 nm and 10 nm programmable bandwidth (Model Varispec VIS-10-20 and SNIR-7-20, Cambridge Research & Instrumentation, Cambridge, MA, USA): the first LCTF covers the visible waveband (400-720 nm) and the second one covers the near infrared waveband (650-1100 nm), a high sensibility monochromatic camera (Model Lumenera LM165) and a 35 mm focal length lens (Model Edmund VIS-NIR NT67-716).

2.2 Hardware and software integration system

The overall configuration of the system hardware is shown in Figure.1 (left). The spectral imager and the illumination system were mounted on two independent stainless steel trolleys in order to facilitate manipulations especially when adjusting orientation above the anatomical tissue. The switched position of the two LCTFs in front of the camera is easily performed by a horizontal rotating bar. The main advantage of the fixed camera is to keep the field of view unchanged when interchanging the visible and the near infrared filters.

The camera and the two filters are controlled by software developed with the MATLAB graphical programming language (MathWorks Inc.) and using the Software Developer Kit (SDK) toolkits provided by the camera and the LCTFs manufacturers. The connection between the computer and the spectral imager is provided through an interactive graphic user interface (GUI) where different parameters can be set (Fig.1 right). Parameters are the wavelength of the filters, the gain and the exposure time of the camera. The software can be operated to acquire multispectral (up to 10 images) and hyperspectral (hundreds of images) images under two modes: either manually or automatically.

The first mode allows a manual adjustment of parameters through interactive sliders while the live video stream is displayed on the GUI window of the software. This mode is useful if the user wants to acquire only few multispectral images. In the second operating mode of software, hyperspectral image acquisition is automatically performed. In this mode, there are two methods: the first method with scan mode that aims to test all the possible combinations using the parameters provided in the three columns of a command window and the second method with sequence mode that aims to test only particular parameter triplets saved into a script file. The acquired hyperspectral image files are automatically named and saved into the specified path. During the two acquisition modes, each acquired mono-band image is displayed on live with the pre-defined parameters, on the computer screen. Several complementary functions are provided in the software to improve the interface usability and to avoid user errors.

2.3 Calibration of the hyperspectral prototype

Designing a hyperspectral system is a comprehensive process of selecting optical, electronic and mechanical elements. Thus, a calibration step is essential to characterize the overall system performance and each of its components. To calibrate the prototype, a series of tests was carried out in both spatial and spectral domains. The different calibration tests and the components used in our experiments are illustrated in the Figure 2.

Figure 1. Hyperspectral imaging prototype (left). The interactive graphic user interface with camera and LCTFs control pushbuttons and different acquisition modes (right).

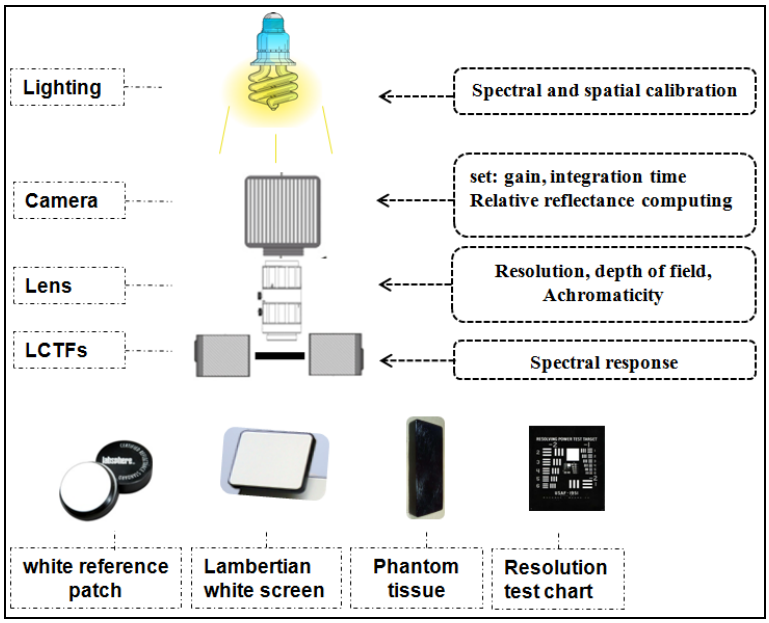

Figure 2. Different calibration tests performed on each component of our hyperspectral system prototype. Elements used in the experiments are shown in the bottom of the figure.

2.3.1. Calibration in the spectral domain

The spectral model used for our prototype is described in equation (1). In such model, each spectral response of all the elements involved in the acquisition process is decomposed. It aims to characterize the reflectance information. By using this model, the signal d_k observed at the camera output, depending on the k^{th} channel, is given by the following equation:

$$d_k = \int_{\lambda\min}^{\lambda\max} I(\lambda)\,\phi_k(\lambda)\,r(\lambda)\,O(\lambda)\,\alpha(\lambda)\,d\lambda \qquad (1)$$

Where I(λ) is the spectral radiance of the illuminant, Φ(λ) is the spectral transmittance of the k^{th} filter, r(λ) is the spectral reflectance (white reference patch, anatomical structure), O(λ) is the spectral transmittance of the optical system (lens) and α(λ) is the spectral sensitivity of the camera. We note that λ_{min} and λ_{max} refer to the interval of transmittance in the k^{th} position of the LCTF.

We performed a pre-processing step for the acquired hyperspectral images by calculating the relative reflectance. This step will correct the significant signal variations, which are caused by the non-uniformity of the illumination and the focal plane array of the camera, known as pattern noise[11, 14]. Using white reference and dark images, the raw spectral images were converted to percentage spectral images. White reflectance images were acquired by our prototype hyperspectral imaging system using 99% Spectralon diffuse reflectance standard (Model SRS-99-010, Labsphere, Inc., North Sutton, NH, USA). Dark images that store the camera internal noises caused by the dark current were acquired by keeping the camera shutter closed. White reference and dark images were acquired with the same spectral and spatial conditions as the final calibrated spectral images. The relative reflectance was calculated using the following equation:

$$R = 100 \times \frac{I - D}{W - D} \tag{2}$$

Where R is the converted relative reflectance image, I is the raw spectral image, D is the dark current image and W is the white reference image.

The spectral sensitivity of the complete image acquisition chain was measured with a white reference patch placed on the camera optical axis over the visible and near infrared band from 400 to 1100 nm with 5 nm increments. For this test, we scanned the 99% Spectralon diffuse reflectance standard after adjusting the camera exposure time in order to avoid either saturated or too dark pixels in the acquired images. The system's sensitivity was determined by calculating the mean intensity extracted from a 250 x 250 pixels ROI on the center of the patch. As we also dispose of the spectral specifications of the camera, the front lens and the LCTFs from manufacturer datasheets, we could verify that our results comply with these data. The spectral response of the illumination system was obtained by using a solarimeter (Model Solrad). Other spectral characteristics of the prototype such as the system spectral accuracy and resolution were measured and fixed by the LCTF manufacturer. In fact, the tuning accuracy specification of the LCTF is that the error on the center wavelength should be less than the actual bandwidth divided by 8 plus 0.5 nm. The spectral resolution is determined from the full-width at half-maximum (FWHM), measured as the spectral separation between the two points where the LCTF's transmission attains 50% of the peak value. The passband center wavelength is the wavelength midway between these two points. LCTF's bandwidths were set during the design and manufacturing process and are not adjustable by the end-user[15].

2.3.2. Calibration in the spatial domain

A LCTF-based spectral imaging system often displays significant signal variations caused by the non-uniformity of the illumination[11]. In our calibration test, we characterized the spatial distribution of the illumination system. We measured the variation of the energetic flow or irradiance which is the flux per unit area received by a surface. The illumination's irradiance was determined using a solarimeter placed in different lateral and diagonal positions with 2 cm intervals from the center of the light spot. The lighting system was positioned at several operating distances (from 80 cm to 110 cm). The spatial distribution with a Lambertian white screen was also characterized. This calibration considers, on each pixel of the image, the sensitivity of each pixel of the camera. In this test, the non-uniformity of the illumination was taken into account when measuring locally with the white reference patch.

In the following test, we had measured the operating distance. Using two scale rulers placed on a white background, the normal distance from camera to work plane was measured in order to find out the optimal distance to centre a field of 10 x 10 cm which is close to the surgical context requirements. First, the camera lens was set on the maximum aperture and then it was focused as the camera was moved up or down. The spatial resolution of the prototype was measured using a standard USAF 1951 resolution target (Edmund Optics, Inc., Barrington, NJ, USA) placed under the spectral imager, perpendicular to its optical axis and set at the operating distance measured previously. The lens aperture was initially set to F/1.65 then the focus was adjusted in order to have a sharp image resolution. The USAF 1951 resolution chart was scanned using the two LCTFs in the spectral range 400 – 1100 nm with 5 nm increments for centred, lateral and diagonal positions of the resolution target in the camera field.

The lens achromatism was measured using the following protocol: the illumination system was positioned at 1 m from the work plane and the standard USAF 1951 resolution target is placed at the operating distance from the spectral imager. The lens was focused at 425 nm as the images at the first wavelengths were too dark. The lens focusing was then

fixed throughout the test. Hyperspectral images are scanned in the spectral range 425 – 1100 nm with 50 nm increment. Before each acquisition, the working distance was increased or decreased in order to find the best point of sharpness.

The depth of field (DOF) is the distance between the nearest and farthest objects in a scene that appear to the human eye acceptably sharp in an image. In this test, we placed the same standard USAF 1951 resolution target, used in the previous test, in a removable bench. The camera-to-target distance was set to the operating distance measured previously and the lens was set to a fixed focus during the test. We chose a single wavelength to acquire all the images in which the contrast is high. The target was moved with an interval of 0.5 cm upstream and downstream from the point of sharpness measured at the operating distance and an image was acquired at each distance.

2.4 Preclinical experiments

In preceding works, we were interested in processing color and multispectral images in the context of wound assessment in telemedicine environments[7, 10]. In our current research, we aim at carrying out the hyperspectral images in the context of surgical interventions in order to discriminate between different tissues, to detect and to explore some anatomical structures. Before beginning the preclinical experimentations, we had tested our systems performance on a phantom tissue that we had designed. This phantom reproduces the spectral response of human breast tissue. The first preclinical experimentations were performed on pig as it is very close to the human model and commonly applied when carrying out clinical trials. When operating, surgeons need to distinguish some delicate hidden anatomical tissues such as the facial nerve because incising it can cause facial paralysis.

Our objective is to extract the spectral signature of the facial nerve. Hyperspectral images were acquired by our LCTF based visible and near infrared (VIS-NIR) spectral imaging system prototype in the spectral range of 400 – 1100 nm with 5 nm increments. Relative reflectance was calculated using the Eq. (2) in two regions of interest (ROI) in the images: the first ROI was selected to characterize the anatomic structure and the second one was to characterize its surrounding tissues. Each ROI is a 20 x 20 pixels window selected using medical expert knowledge in the hyperspectral images.

3. EXPERIMENTAL RESULTS

3.1 Spectral domain

Figure 3 shows the results of the measurements averaged over the white reference patch. The spectral sensitivity of the complete acquisition chain is plotted. It is in accordance with the spectral curves of the spectral imager and the illumination system provided in the manufacturer's datasheets. The typical shape of the curve illustrates the fact that when reaching the lower or upper limits of the bandpass, the camera sensitivity drops and so is the power of the lighting. This is slightly compensated by the LCTFs spectral response which increases with the wavelength[15]. For each LCTF, we had fixed three integration times so that the pixel intensity in the acquired image is constrained between 50 and 240 (Tab.1). The exposure times are compatible with video frame rates with the exception of wavelengths over 1020 nm where the sensor's sensitivity is very low.

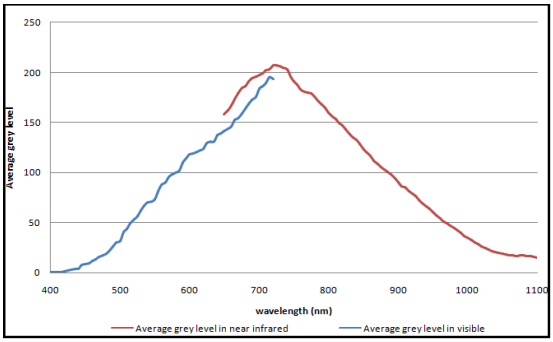

Figure 3. Averaged intensity of a 250 x 250 pixels ROI on the white reference patch with 5 nm increments in the spectral range. The first LCTF in visible 400 – 720 nm (blue). The second LCTF in near infrared 650 – 1100 nm (red).

Table 1. Integration time setting for visible and near infrared LCTFs in order to obtain grey level values between 50 and 250 over the white reference patch.

LCTF	**VIS**			**NIR**		
Wavelength (nm)	400-460	465-525	530-720	650-920	925-1015	1020-1100
Integration time (ms)	22	4	1.33	4	15	66

3.2 Spatial domain

The curves in Figure 4 show that for a distance of 1 m between the illumination system and the operating field, illumination decreases by 70% between the center and the edge. On the other hand, we conclude that illumination increases as the distance between the lighting system and the solarimeter decreases. For a distance above 90 cm, the illumination values for diagonal positions of the solarimeter are greater than those registered for the lateral positions. In addition, we note that there is a small variation of the illumination between the lateral and the diagonal position of the object to be illuminated. Then, it has been proved that the uniformity of the lighting is acceptable over the camera field of view and as we had adopted a sufficient dynamic (256 gray levels) to properly visualize different tissues reflectances at the center or at the edge of the image.

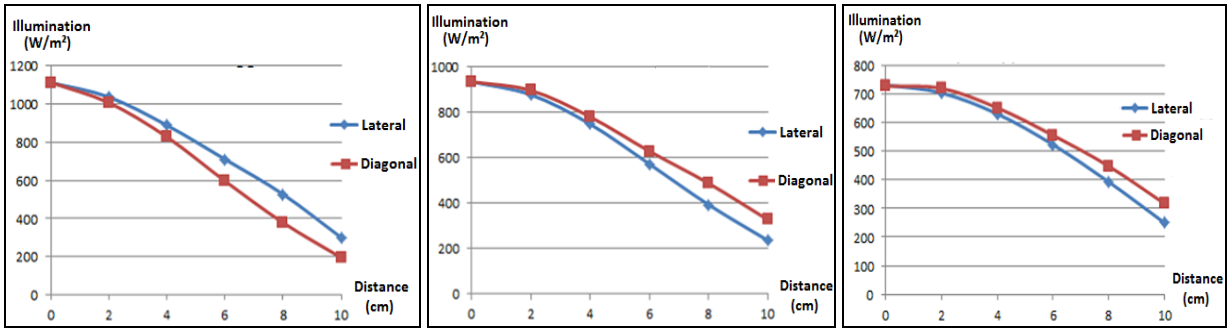

Figure 4. Irradiance of the illumination system placed in different distance from the solarimeter: (a) 90 cm, (b) 100 cm and (c) 110 cm.

The operating distance was measured to be 45.2 cm. It is the optimal camera-to-subject distance in order to have approximately a field of 10 x 10 cm which is well scaled to the surgical field. The real field imaged by the camera was calculated to be 11 cm x 8.2 cm. We conclude that, in a feasibility phase, this distance is acceptable as the camera should not cause obstruction when surgeon is operating. By removing the camera for a higher distance, the focal length will be increased however it will lead to a smaller depth of field.

The spatial resolution of the system was determined using the group number of the recognized discernible ruling set in the standard USAF 1951 resolution target where each ruling element has three identical black bars separated by two white bars. The system spatial resolution is measured in line pairs per millimeter (lp/mm) by referring to the look up table of the test resolution target [13]. The line pair (lp) means a black and a white line. Results are represented in Table 2. It shows that the system's spatial resolution varies between 5.04 lp/mm and 6.35 lp/mm. This difference is due to the sensitive focus of the lens set on the maximal aperture. Those results are compared to the camera's pixel resolution 1392x1040 pixels for a field of 82 x 110 mm. Thus, the pixel resolution is 0,079 mm.pixels^{-1} yielding a spatial resolution of 13 pixels.mm^{-1}. It is showed in Table 2 that for a central position and when increasing the lens aperture, both spatial resolution and depth of field decreased. We also conclude that the spatial resolution is theoretically reduced with the wavelength for physical reasons. The central position is adopted in order to ensure better resolution, lower distortion of the camera lens and higher lighting brightness.

Figure 5 shows the resolution of the system for different camera-to-target distances. The depth of field is determined where the spectral imager resolution was greater than 50% of the maximum value. The experimental curve indicates that the system's depth of field is 4 cm. In other word, the main shift on either sides of the operating distance is measured to be ± 2 cm. This distance is estimated as the strict minimum adequate distance in order to observe some tissues with an important shape.

Table 2. Spatial resolution of the spectral imager system measured using the standard USAF 1951 resolution target placed in central, lateral and diagonal positions.

	Central	Central	Central	Central	Lateral	Diagonal
Wavelength *(nm)*	900	650	650	650	650	650
Aperture	F/1.65	F/8	F/1.65	F/1.65	F/1.65	F/1.65
LCTF	SNIR	SNIR	VIS	SNIR	SNIR	SNIR
Resolution *(lp/mm)*	5.04	6.35	5.66	5.35	5.04	5.66

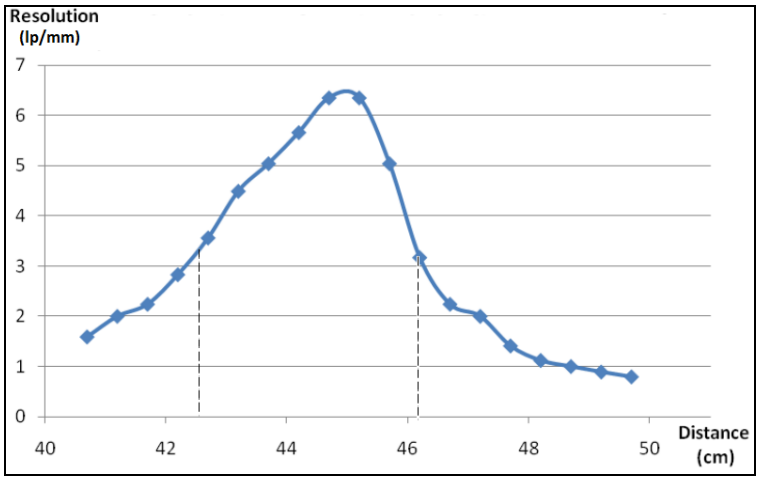

Figure 5. The depth of field is based on the interval where the spectral imager resolution is greater than 50% of the maximum value.

Figure 6 shows that there is chromatic softness caused by the lens throughout the different wavelengths. A linear and horizontal curve is expected from the first operating distance (45.2 cm) where the lens is focused. However, we note that the distance is varied in the spectral range 425 – 1100 nm. Then, in order to avoid acquiring blurred images, the lens focus had to be adjusted when changing between the two LCTFs.

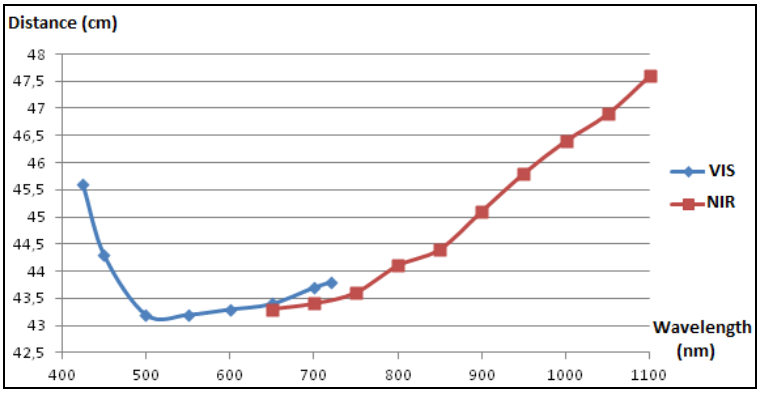

Figure 6. The achromatism of the lens measured in the spectral range of 425 – 1100 nm with 50 nm increments

3.3 Results of preclinical experiments

The first preclinical experiments were carried out during a parotidectomy on pig in order to explore some anatomical tissues like the facial nerve (Figure 7 right) in visible and near infrared spectral range. The spectral signature of the anatomical tissue and its surrounding were calculated and characterized from the hyperspectral cube. Figure 7 (left)

shows the relative reflectance of the facial nerve and its surrounding tissue plotted in 400 – 1100 nm. We conclude that the spectrum of the facial nerve showed a higher reflectance than the spectrum of its surrounding tissue. We note that in the spectral region of near infrared 650 – 850 nm, both spectra showed great disparities (12 – 23%) while there is a small reflectance difference (less than 10%) between both spectra in visible spectrum range 400 – 600 nm. Thus, using the spectral signature extracted from the collected hyperspectral images, anatomical tissues are distinguishable in near infrared spectral domain where there is difficulties for the naked eye surgeon. As the human vision covers the spectral range of 400-780 nm we can say that the surgeon, based on his anatomical knowledge, should be able to view the tissues in the visible range of the spectral gap between the reflectance curves. However, the human vision has only three wide and overlapping channels that are schematically focused on red, green and blue channels while the hyperspectral system can acquire hundreds of disjoint and fine channels. These results demonstrated the advantage of using the LCTF based spectral imaging system in operating room.

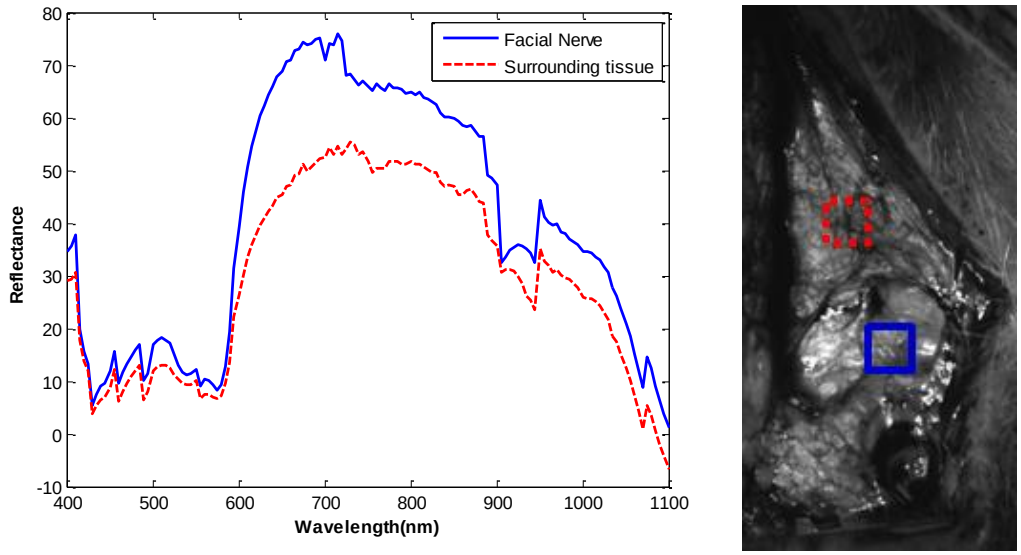

Figure 7. Parotidectomy on a porcine model. The bold blue window is on the facial nerve and the dotted red window is on the surrounding tissue (right). Spectral characterization of the facial nerve and its surrounding in the spectral range 400 – 1100 nm (left).

4. CONCLUSION

In this paper, we had evaluated the performance of a new hyperspectral imaging prototype in visible and near infrared spectral range (400 – 1100 nm). Our LCTF based spectral imaging system was calibrated in both spatial and spectral domains. The calibration and characterization steps were followed by preclinical surgical interventions. It results that multispectral and hyperspectral imaging is a new modality that can be easily integrated in operating rooms with very little disturbance. We note mainly the lens achromatism when changing between the two LCTFs. Other lens is considered to be tested to avoid some vignetting effects. By providing tissue spectral characteristics, many anatomical tissues could be differentiated in spectral range where the naked eye's performance is surpassed. Further exploration will be carried out in the medium infrared band which is promising for medical applications by testing a high resolution InGaAs camera (900-1700 nm).

ACKNOWLEDGMENTS

The authors would like to thank the French Conseil Régional Centre, and Ministère de l'Industrie, the European fund for regional development (FEDER) and the French OSéO for their financial support through the smart electricity cluster S2E2.

REFERENCES

[1] Akbari, H. and Kosugi, Y., "Hyperspectral imaging: a new modality in surgery," Recent Advances in Biomedical Engineering, Ganesh R Naik (Ed.), ISBN: 978-953-307-004-9 (2009).

[2] Akbari, H., Uto K., Kosugi Y., Kojima K. and Tnaka, N., "Cancer detection using infrared hyperspectral imaging," Cancer Science, Vol. 102 n°4, 852-857 (2011).

[3] Choudhary, R., Mahesh, S., Paliwal, J. and Jayas, D.S., "Identification of wheat class using wavelet features from near infrared hyperspectral images of wheat kernels," Biosystems Engineering 102(2), 115-127 (2009).

[4] Jayapala, M., Compact high-speed & low cost hyperspectral imaging for biomedical applications, IMEC Leuven Belgium SSET/NVISION report 8-10, Stuttgart Germany (2011).

[5] Jolivot, R., Nugroho, H., Vabres, P., Fadzil, M. H. A. and Marzani, F., "Validation of a 2D multispectral camera: application to dermatology/cosmetology on a population covering five skin phototypes," European Conferences on Biomedical Optics, Munich, Germany (2011).

[6] Liu, X., Setiadi, A. F., Alber, M. S., Lee P. P. and Chen, D. Z., "Identification and classification of cells in multispectral microscopy images of lymph nodes," Proc. SPIE 7962, 79620J (2011).

[7] Nouri, D., Lucas, Y. and Treuillet, S., "Comparaison de deux approches supervisée et non supervisée pour évaluer la cicatrisation d'une plaie," Sciences of Electronics, Tech. of Inform. and Telecom. SETIT, Tunisia (2012).

[8] Shippert, P., Introduction to Hyperspectral Image Analysis, Research Systems, Inc., Issue No. 3: Remote Sensing of Earth via Satellite (2003).

[9] Qi, X., Xing, F., Foran, D. J. and Yang, L., "Comparative performance analysis of stained histopathology specimens using RGB and multispectral imaging," Proc. SPIE 7963, 79633B (2011).

[10] Wannous, H., Lucas, Y. and Treuillet, S., "Robust tissue classification for reproducible wound assessment in telemedicine environments," Journal of Electronic Imaging 19, 023002 (2010).

[11] Wang, W., Li, C., Tollner, E.W., Rains, G. and Gitaitis, R., "A liquid crystal tunable filter based shortwave infrared spectral imaging system: Calibration and characterization," Computers and Electronics in Agriculture, Volume 80, 135-144 (2012).

[12] Zuzak, K., Francis, R., Smith, J., Tracy, C., Cadeddu, J. and Livingston, E., "Novel hyperspectral imager aids surgeons" Proc. SPIE Newsroom 10.1117/2.1200812.1394, 3 (2008).

[13]Wikipedia, 1951 USAF resolution test chart, Retrieved December 5 2012, http://en.wikipedia.org/wiki/1951_USAF_resolution_test_chart>.

[14] Chang, C.-I., [Hyperspectral Data Exploitation: Theory and Applications], Wiley Interscience, Hoboken (2007).

[15] CRI, VariSpec Liquid Crystal Tunable Filters User's Manual, MD15474 Rev. D, Woburn, MA, USA (2010).

[16] Gat, N., "Imaging spectroscopy using tunable filters: A review," Proc. SPIE 4056, 50–64 (2000).

[17] Panasyuk, S. V. et al., "Medical hyperspectral imaging to facilitate residual tumor identification during surgery," Cancer Biology & Therapy, 6(3), 439–446 (2007).

[18] Goetz, A. F. H., "Three decades of hyperspectral remote sensing of the earth: a personal view," Remote Sensing of Environment, 113(Suppl. 1), S5–S16 (2009).

[19] Sun, D.-W., [Hyperspectral Imaging for Food Quality Analysis and Control], Academic Press, Elsevier Science & Technology, Burlington, MA, USA, (2010).

[20] Akbari, H. et al., "Detection and analysis of the intestinal ischemia using visible and invisible hyperspectral imaging," IEEE Trans. Biomed., Eng. 57(8), 2011–2017 (2010).